-RESEARCH PAPER-

International Journal of Mining and Geo-Engineering

IJMGE

IJMGE 57-3 (2023) 305-313

DOI: 10.22059/IJMGE.2023.354353.595027

Integrated interpretation of aeromagnetic and aero-radiometric data to delineate structures and hydrothermal alteration zones associated with Gold and Base metal Mineralization in Chitipa area, Northern Malawi

Joshua Chisambi [a, *], Tiyamike Haundi [a] and Steven Ghambi [a]

[a] *Department of Mining Engineering, Malawi University of Business and Applied Sciences, Blantyre, Malawi.*

Article History:

Received: 25 January 2023.

Revised: 11 May 2023.

Accepted: 08 June 2023.

ABSTRACT

An analysis of aeromagnetic and aero-radiometric data from the Chitipa area in northern Malawi is presented in this study. The aim is to delineate structures, hydrothermal alteration areas, and gold mineral potential zones, as well as to identify regions suitable for further mineral exploration. Airborne geophysical data, specifically aeromagnetic and aero-radiometric data, were employed. Several enhancement techniques and filters were applied to the geophysical data, including reduction to the pole, computation of the first vertical derivatives, analytical signal processing, tilt angle derivative enhancements, Centre for Exploration Targeting (CET) grid analysis, Euler deconvolution, and radiometric data ratios. The results of the analysis offer detailed insights into the subsurface geology. It is indicated that the area is characterized by faulting and shearing, with structures predominantly trending in a northwest direction. Minor trends in the northeast-southwest, east-west, and north-south directions were also observed. Zones with hydrothermal alteration were discovered to coincide with structural associations in the NW part of the study area, suggesting that the structures served as channels for migrating hydrothermal fluids that reacted with the rock formation, resulting in alteration. The northwest area is identified as a promising mineralization zone, emphasizing the need for further exploration efforts in this region.

Keywords: *Gold and base metal, Mineralisation, Chitipa, Mineral exploration, Airborne geophysics.*

1. Introduction

A significant portion of the world's gold production originates from orogenic gold deposits, which form along convergent plate boundaries during compressional to transpressional deformation processes. These deposits are globally distributed within belts of locally metamorphosed rocks situated in proximity to crustal-scale shear zones [1]–[3]. Strong structural controls play a pivotal role in governing mineralization, typically occurring within second or third-order structures. These structures are instrumental in localizing mineralization, serving as conduits for hydrothermal fluids. Geophysical measurements are imperative for assessing such deposits [4] [1].

It is customary to employ geophysical techniques, especially high-resolution magnetic and aero-radiometric methods, to map concealed geological structures directly linked to mineralization [4]. These techniques are widely adopted worldwide as foundational tools for geological interpretations since they are instrumental in defining geological features such as faults, folds, shear zones, and other favorable locations for mineralization [4]–[8].

Before embarking on any interpretation, the magnetic data must undergo certain enhancements. These enhancements may encompass the analytic signal technique [9], horizontal gradient, continuous wavelet transforms of horizontal derivatives in potential field data, tilt angle derivatives, and CET grid analysis—an automated approach for detecting lineaments from field data. Aeromagnetic data has been employed to detect geologic structures in orogenic gold deposits [4]–[8], [10]–[12].

Gamma-ray spectrometry, on the other hand, examines the distribution of radioelements (K, Th, U) on the Earth's surface. Due to variations in the concentrations of these radioelements in different rock types, gamma-ray spectrometry can be employed to map and classify various lithological units [13]–[16]. When compared to other airborne geophysical methods, aero-radiometric mapping exhibits a higher rate of success in geological surface mapping [17]–[19]. Several studies involving the remapping of lithological units using this approach have been conducted (e.g., authors in [14], [20]–[26]).

Furthermore, this approach proves highly effective and accurate in identifying hydrothermal alteration zones. According to Shives et al. [27], the eTh/K ratio provides the best indication for detecting potassic alteration zones. Moreover, it can be used to deduce certain structures that might otherwise remain undetected.

Hence, aero-magnetic and aero-radiometric data can be employed to assess structural properties and identify hydrothermal alteration zones, as demonstrated by studies conducted by authors in [28], [29]. Researchers, such as those mentioned in [4]–[8], [10]–[12], have utilized aero-radiometric and magnetic data effectively to identify geological structures within orogenic gold deposits. In a similar vein, authors in [30] evaluated the geological structural patterns of the Kirk Range in Malawi using a combination of aerial magnetics and aero-radiometric data. Their findings unveiled various geological units with the potential for gold deposit mineralization, including contact zones and hydrothermal alteration zones.

Through the utilization of an integrated remote and aeromagnetic dataset, Eldosouky et al. [11] conducted an analysis to identify structural

* Corresponding author: *E-mail address:* jchisambi@poly.ac.mw (J. Chisambi).

characteristics and hydrothermal alteration zones within Egypt's south eastern desert. Based on the outcomes of their investigation, the authors created maps and made predictions regarding locations with significant mineral potential.

Similarly, using gamma-ray, magnetic, and remote sensing data from the Western Safaga area in the eastern desert of Egypt, Ahmed [31] detected anomalous radioactive zones closely associated with mineral deposits. Subsequently, they compiled a comprehensive map of the region, encompassing geological features, structural aspects, hydrothermally altered zones, and mineralization zones.

In Malawi, despite the presence of abundant mineral resources, there has been relatively limited geophysical exploration conducted in the country. This is evident from the fact that many local Malawians engage in mineral extraction activities, such as extracting gold from quartz veins and placer deposits in various areas across the nation. One of the regions where artisanal gold mining is prevalent is Chitipa district in northern Malawi. Although Malawi boasts numerous gold occurrences, the precise structural factors governing primary mineralization remain largely unknown. This knowledge gap is primarily a result of the limited research conducted in the country.

Recently, the Malawi government has taken a significant step forward by acquiring high-resolution airborne geophysical data covering the entire country. The objective is to unlock the mineral potential of Malawi. In this study, we analyse the newly acquired aeromagnetic and aero-radiometric data for Chitipa in northern Malawi. Our aim is to delineate geological structures and hydrothermal alteration zones, as well as to identify areas with potential for gold and base metal mineralization. Furthermore, we seek to pinpoint promising regions for further mineral exploration. Conducting this type of study will enhance our understanding of the structural controls influencing gold mineralization. It will also serve as a valuable reference for future gold exploration in the Chitipa area and other similar regions within Malawi.

2. Regional Geology

The geology of Chitipa and the entire nation of Malawi remains relatively understudied, with the most recent geological map dating back to 1965 [32]. The geological composition of Malawi is primarily characterized by high-grade para- and orthogneiss metamorphic rocks originating from the Precambrian and Paleozoic eras, collectively known as the Malawi basement complex rocks [33]. These basement complex rocks have undergone significant transformations, including extensive metamorphism and multiple phases of deformation [34], [35]. They hold a long history of structural and metamorphic activity and are associated with three major mountain-building events, namely the Ubendian, Irumide, and Mozambiquean orogenies [36], [37].

The Ubendian orogeny, responsible for NW-SE trending structures primarily confined to the northern regions of Malawi, signifies the amalgamation of eastern African and Archean cratonic blocks/nuclei [38], [39], [40]. Another consequential tectonic and metamorphic event, the Irumide orogeny, gave rise to the Irumide belt. This belt extends from Zambia, traverses central and southern Malawi, and extends into northern Mozambique [41]–[43]. The principal structural orientation within the Irumide belt is NE-SW, owing to significant crustal compression during the primary phase of the Irumide orogeny [44]–[46].

The formation of the Mozambique Belt can be attributed to the Pan-African Orogeny, which took place approximately 800 to 500 million years ago [40], [46]. This event represents the most recent significant orogenic activity impacting the geological history of Malawi. It led to the modification of older orogenic features stemming from the Ubendian and Irumide orogenies [47]. As a result, predominantly north-south-oriented structures and textures emerged. During the Pan-African Orogeny, the highest metamorphic conditions occurred, with peak temperatures reaching 750-800°C and pressures around 12-13 kbar. Subsequently, there was a transition to amphibolite facies, characterized by temperatures of 550-700°C and pressures of 5-8 kbar [49] [48]. This Pan-African tectonic activity and high-grade metamorphism brought about significant changes and reactivations of pre-existing structures from earlier orogenic periods, including the Ubendian, Irumide, and Kuunga [49]. This process led to the formation of predominantly north-south trending structures and fabrics. Importantly, it's worth noting that Kröner and Collins determined that during the Pan-African overprinting, the high-grade gneiss assemblage in Malawi experienced peak metamorphic conditions at temperatures of 900 ± 70°C and pressures of 9.5 ± 1.5 kbar [50]. Figure 1 presents a geological map of the region.

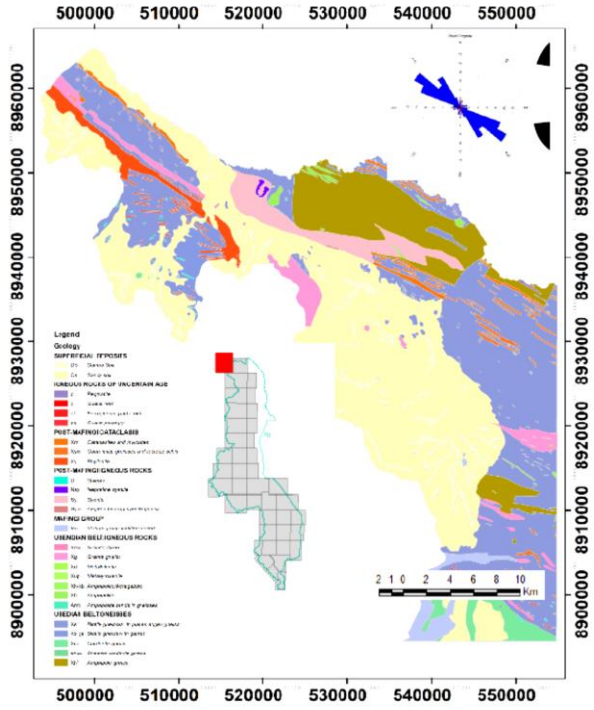

Figure 1: Regional geology map for the study area, insert is the index map of Malawi and the red square is the location of the study area (Source: Geological Survey of Malawi).

3. Materials and Methods

3.1. Aeromagnetic data

Data acquisition and preparation

The Geological Survey of Malawi (GSM) supplied the aeromagnetic and aero-radiometric data utilized in this study. The magnetic data was collected between 2012 and 2013 by Sander Geophysics on behalf of the Malawi government, using Scintrex Cesium vapor magnetometers installed on a Cessna Caravan fixed-wing aircraft, flying at an altitude of 80 meters with terrain clearance and line spacing set at 200 meters apart. The flight lines followed a NE-SW orientation, with tie line spacing set at 2000 meters. Data processing employed the WGS 84 Datum and Universal Transverse Mercator (UTM) map projection technique.

The aeromagnetic data underwent processing to remove regional anomalies, utilizing the International Geomagnetic Reference Field (IGRF 2010). To identify magnetic anomalies above their source bodies and eliminate the skewness of the anomalies, we reduced the total magnetic intensity map to the pole (RTP), following the approach recommended by Baranov [51]. The magnetic field's inclination (50°) and declination (-7°) were employed to create the RTP map (refer to Fig. 2).

Subsequently, several enhancement and filtering procedures were applied to the resulting RTP map, enhancing data interpretability. Specifically, we employed the first vertical derivatives, the analytical signal, and the tilt angle derivative enhancements in this study. These

filters furnished additional insights and revealed specific structural traits crucial for interpretation purposes. The data processing was conducted using Oasis Montaj Geosoft software [52].

First Vertical Derivatives

When computing the first vertical derivative of aeromagnetic data, it serves to accentuate magnetic sources near the surface and enhances the resolution of closely positioned sources, as noted in previous studies [53]–[57]. This process specifically amplifies short-wavelength anomalies while diminishing long-wavelength ones, thus highlighting shallow features such as boundaries and associated lineaments. Nabighian's [9] first vertical derivative, expressed as follows, was employed for this purpose:

$$\mathrm{FVD} = \frac{\partial T}{\partial z} \tag{1}$$

Analytic signal and Tilt derivative

The analytical signal (ASIG) technique, as introduced by Nabighian [9], is employed to emphasize peak responses above magnetic anomalies. This method is commonly used in regions with low magnetic latitudes due to the inherent complexities associated with the reduced-to-pole operation. The application of the analytic signal filter is intended to enhance magnetic discontinuities and reveal the boundaries of anomalies [58]. According to Nabighian [9], the formula for the analytic signal is as follows:

$$\mathrm{AS}(x,y) = \sqrt{\left(\frac{\partial T}{\partial x}\right)^2 + \left(\frac{\partial T}{\partial y}\right)^2 + \left(\frac{\partial T}{\partial z}\right)^2} \tag{2}$$

where T is the observed magnetic anomaly and $\frac{\partial \mathrm{T}}{\partial \mathrm{x}}, \frac{\partial \mathrm{T}}{\partial \mathrm{y}}, \frac{\partial \mathrm{T}}{\partial \mathrm{z}}$ are the orthogonal horizontal derivatives of the magnetic field in x, y, and z of the magnetic data respectively.

The tilt angle derivative (TDR) is employed to illustrate the boundaries of geological structures. TDR is defined as the mathematical ratio between the vertical and horizontal derivatives of anomalies, and it is expressed as:

$$\theta = \tan^{-1} = \frac{\frac{\partial^2 A}{\partial z^2}}{THD_{(x,y)}} \tag{3}$$

Euler deconvolution

The Euler deconvolution method was employed to evaluate the depth of magnetic sources in the research area. This approach, founded on the Euler homogeneous equation (iv), characterizes the geometry of magnetic bodies using structural indices (SI) [60].

$$(x - x_0)\frac{\partial T}{\partial x} + (y - y_0)\frac{\partial T}{\partial y} + (z - z_0)\frac{\partial T}{\partial z} = N(B - T) \tag{4}$$

The equation represents the relationship between a magnetic source located at coordinates (x_0, y_0, z_0) and the total magnetic field observed at coordinates (x, y, z). The derivatives $(x, y, z), \frac{\partial T}{\partial x}\frac{\partial T}{\partial y}$ and $\frac{\partial T}{\partial z}$ represent the rate of change of the magnetic field in the x, y, and z directions, respectively. B is the regional value of the total magnetic field. The degree of homogeneity, N, is used as a measure of the structural index [61]. The attenuation rate of an anomaly at a particular observation point is determined by the Structural Index (SI), which is influenced by the characteristics of the field source. The Euler deconvolution solutions were calculated using RTP aeromagnetic data. Structural indices of 0, 0.5, 1, 2, and 3, were applied, along with a window size of 10 x 10. "A window size of 10 × 10" means a squared window with a dimension of 10*50 m=500m (10×cell size).

Analysis of the Centre for Exploration Targeting grid (CET)

The CET Grid Analysis, an Oasis montaj™ add-on, is designed for exploration targeting, as described in [52]. CET consists of algorithms that automatically delineate lineaments and identify promising ore deposit areas. The CET Grid Analysis extension includes tools for analyzing textures, phases, and structures in gridded data using various statistical processes such as texture analysis, lineation delineation, vectorization, and structural complexity analysis. In our study, we used this extension for grid texture analysis, lineament detection, edge detection, threshold identification, and heatmap generation.

3.2. Aero-radiometric data

The aero-radiometric data were gridded to produce maps illustrating surface distributions of potassium, equivalent thorium, and equivalent uranium. This aero-radiometric method proves highly useful for identifying hydrothermal alteration zones and mapping lithological units. The enhancement operations utilized potassium (K), equivalent thorium (eTh ppm), equivalent uranium (eU), and ternary imageries [17], [62]. These operations resulted in maps that correlate with the pattern and trend of geological units [27]. Additionally, a Th/K ratio map was created to aid in the mapping of hydrothermal alteration zones, as a decrease in eTh and an increase in K signify alteration conditions in an ore deposit [63]. Lastly, a ternary map was generated by combining the three radioelements, potassium, thorium, and uranium, using RGB colours.

4. Results and Discussion

4.1. Airborne Geophysics

Magnetic Survey and Data Interpretations

Figure 2 presents the results obtained from the preliminary analysis of the magnetic susceptibility data. The Reduced to Pole (RTP) map (Fig.2a) illustrates that the research area is characterized by a wide range of values. These values may be categorized into distinct colors based on their amplitudes. Low magnetic anomalies are detected in the northwestern and southwestern regions of the study area, denoted by blue color shades ranging from -315 to -156 nT. They are associated with loose sediments. Intermediate-scale colors, ranging from -119 to -12 nT, are denoted by light green color shades. These colors mostly cover the areas that are located in the center of the image. They are associated with schists. The eastern part of the area under study is covered by the high amplitude anomalies, denoted by magenta color shades which fall between 18 and 215 nT and strikes in the NW-SE direction. They are associated with biotite and granitic gneiss lithologic facies.

The results of the First Vertical and Tilt Derivative filtering approach are depicted in (Fig. 2b). The data filtration reveals that the north western and south eastern portions of the study area display short-wavelength anomalies, suggesting shallower depths of causative sources when compared to the central part of the region. This area is characterized by faulting, and the long linear features are interpreted as significant fractures or faults. These structures predominantly trend in the northwest direction.

To identify linear structures, the RTP map underwent CET grid analysis, following the methods outlined in the "CET grid analysis approach." Textural analysis, phase symmetry, and amplitude thresholding were employed to enhance lineaments, to generate the vectorization lineament map. The distribution of lineaments extracted through CET is presented in (Figs. 2c and d). The area is characterized by faulting, thus the long linear features are interpreted as major fractures/faults with a predominant NW trend. These fractures, shear zones, and faults may have served as conduits for hydrothermal solutions or magmatic activities, which could have led to mineralization emplacement. This pattern signifies fractures and faults impacting the basement complex, indicating the influence of deep crustal heterogeneity. The primary lineament trend corresponds to the Ubendian deformational episode in the study area. Ubendian deformation was the dominant force in the study area and affected northern Malawi. Furthermore, upon examining the vectorization map (Fig. 2d), it becomes evident that the northwestern and southeastern portions of the area's basement rocks have experienced significant deformation. Collectively, these results provide crucial insights into the

basement fractures and faults that have affected this region.

The identification of the contacts and boundaries of magnetic source bodies was accomplished by applying the AS interpretation method (Fig. 2e). These were identified as magnetic highs or lows in specific study area locations. The AS map exhibits two different magnetic zones and a linear dyke in the western part. The zones of high magnetic anomalies (HM) in the north western and south-eastern parts are related to biotite and granitic gneiss. The moderate-intensity domain at the centre is associated with schists; Anda low-magnetic region is associated with loose sediments.

These anomalies appear to be predominantly controlled by structural factors, primarily trending in the NW–SE direction. The zones with low amplitude magnetic signatures are indicative of suspected hydrothermal alteration areas. This is due to the fact that hydrothermal fluids cause magnetic minerals in the rocks they pass through to lose their magnetic properties, resulting in permanent demagnetization, as noted in references [64] and [65]. On the other hand, the zones displaying low- and intermediate-magnetic intensity may represent reflections of downfaulted blocks within the basement complex.

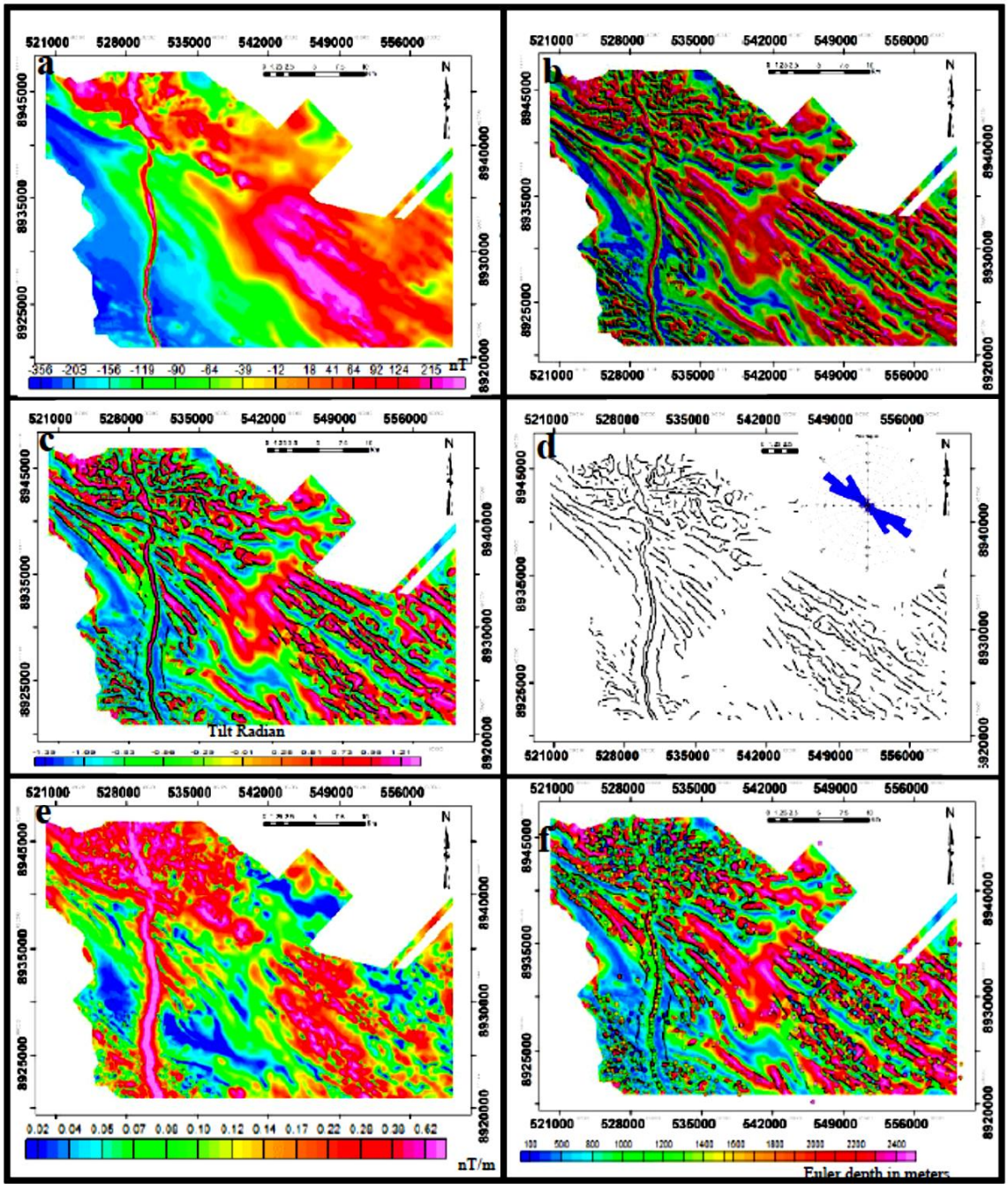

Figure 2. (a) Reduced to Pole Total Magnetic Intensity map. b) Tilt derivative map colour shaded (c) Delineated faults (black lines) overlain on the tilt derivative map. (d) Vectorised map derived from CET grid analysis depicting faults as linear fractures that mostly trending in NW-SE direction (e) Analytical signal map. (f) Euler solutions have been overlain on the tilt derivative map and most solutions fall on linear structures (faults, the black lines indicate faults.

Additionally, the map displays magnetic discontinuities that could potentially serve as indicators of fracture zones for mineral prospecting. Furthermore, the Euler deconvolution technique by Nabighian [9] and Reed [66] found application in determining the depth to the magnetic basement through the utilization of the Euler equation on the RTP magnetic data. As per the Euler deconvolution analysis, the depth to magnetic sources spanned from 270 to 2800 meters (see Fig. 2f). The range of 270 to 900 meters within the basement rocks signifies shallower magnetic sources, while the depth range of 1000 to 2800 meters points to deeper sources. As displayed in Figure 2f, the solutions cluster along the geological lineaments observed on the Tilt derivative map

The primary structural trends inferred from the magnetic data reveal fracture and fault zones trending in a northwest to southeast direction. The majority of these structures appear to lie within the depth range of 300 to 2900 meters. These features are believed to represent samples of large-scale structural fractures within the study region, potentially facilitating the unhindered movement of mineralizing fluids. They may also be associated with economically significant gold mineralization.

A lineament density map, created from the extracted trends, displays areas of high structural density. The structural complexity is visualized using heat maps that highlight regions with structural intricacies. The generation of the structural complexity heat map was achieved through the application of Centre for Exploration Targeting (CET) grid analysis.

In the heat map shown in Fig.3b, areas potentially featuring complex structures are emphasized. The color scheme provides a clear indication: red signifies areas with a high density of structural complexity, while blue represents areas with minimal structural complexity and density.

These maps collectively demonstrate that the north western (NW) region exhibits a high degree of structural complexity, thereby increasing its potential to support mineralization.

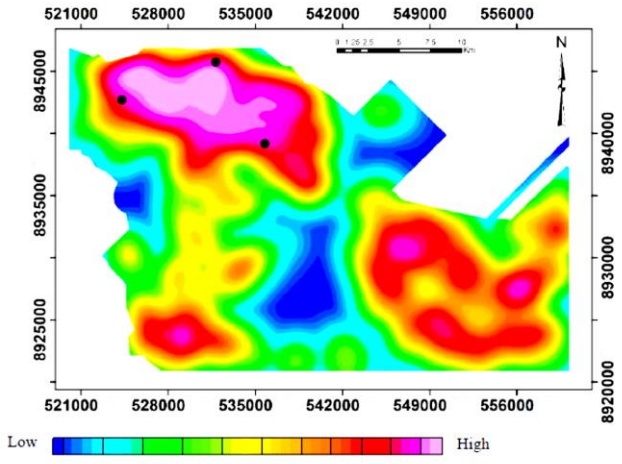

Figure 3: Heat map indicating probable areas likely to contain gold and base metals in red. These delineated areas need further exploration, black dots indicate areas of active gold mining occurrences.

4.2. Radiometric survey and data interpretation

Aero-radiometric data were subjected to interpretation through the use of a potassium (K (%)) map, a thorium (eTh (ppm)) map, an uranium (eU (ppm)) map, and a potassium over thorium (K/Th) ratio map.

In the K map (as seen in Fig. 4a), it is observed that metasediments exhibit high levels of potassium concentration. Metavolcanics, metagabbro, and quartzite rocks, on the other hand, display intermediate levels of potassium concentration. In contrast, amphibolite gneiss and biotite gneiss are associated with relatively low potassium concentrations.

Based on the eth map (Figure 4b), granitic gneiss, quartz reefs, and biotite gneiss are associated with high concentration (HC) levels, while metasediments and metamorphic rocks are associated with intermediate concentrations (IC) and low concentrations (LC).

On the EU map (Fig. 4c), HC values are associated with granitic gneiss, quartz reefs, and biotite gneiss, while low concentrations (LC) and intermediate concentrations (IC) are linked to amphibolite gneiss and metasediments.

Furthermore, radioelement maps demonstrate that the study area is underlain by rocks containing various compositions of radioactive elements, which are aligned in a NE–SW direction. Consequently, the most discernible pattern observed is the NW-SE trend, a well-established feature evident in both aero-radiometric and aeromagnetic maps, thus affirming its significance in the studied region.

Last but not least, the research area was depicted in a ternary map (Fig. 4d), created through equal modulations of the three colours: red (R), green (G), and blue (B). Upon examining this map, it becomes possible to discern lithological disparities resulting from geological and mineral exploration. Across the study area, regions displaying white coloration correspond to zones with high concentrations of radioactive elements. These regions are commonly associated with granites, as indicated by the aero-radiometric response. Meanwhile, the black coloration on the ternary map represents radioactive materials with low concentrations, typically linked to amphibolite gneiss rocks. In the study area, metasediment rocks appear to contain higher K content compared to Th and U content, while the formations of biotite gneiss rocks in the study area exhibit low Th content but high K and U content.

Utilizing the Th/K ratio map proves to be an excellent method for identifying signals associated with zones of hydrothermal alteration. In numerous ore deposits, the presence of hydrothermal alteration can be discerned through a heightened percentage of potassium (K) and a diminished thorium (Th) content. As illustrated in Figure 4e, this Th/K map vividly portrays this relationship. The regions affected by hydrothermal alteration are prominently marked in blue. These modified areas are predominantly concentrated in the north western section, with granitic gneiss and amphibolite gneiss typifying this particular region.

Zones with hydrothermal alteration coincide with structural associations, indicating that these structures served as conduits for the movement of hydrothermal fluids that concurrently interacted with rock formations, leading to alteration. These areas exhibiting hydrothermal alteration align with the lineaments depicted in Fig. 2d and the heat map of the study area in Fig. 3, potentially signifying mineralization zones. Moreover, these zones also follow the NW-SE trend, which corresponds to the preferred direction of the lineaments, suggesting a reasonable likelihood of discovering additional mineralization in this direction. The coexistence of these alteration zones, intricate lineaments, and the heat map strongly implies a high likelihood of gold mineralization occurrence. Consequently, these regions represent high-potential zones for mineralization and warrant prospecting efforts. The prediction and mapping of new areas with high-probability mineral resources are facilitated by the clear alignment between the density maps and the strong correlation between mineralization sites in the study area and the underlying structures.

5. Conclusion

Aeromagnetic and aero-radiometric data were employed to identify geological characteristics and potential gold and base metal exploration locations. The study's conclusion indicates that the area is highly fractured, with NW-SE trending fractures serving as channels for hydrothermal fluids that have altered the surrounding rocks, rendering them potential targets for concealed gold and base metal exploration. Zones featuring hydrothermal alteration, identified using the Th/K ratio, coincide with a structural association and heat maps in the NW part of the study area. This region is characterized by prevalent artisanal mining, and a strong correlation is observed between artisanal mining occurrences and the promising exploration target areas identified in this study. The correlation between indicated target areas, interpreted structures, and active artisanal mine locations in the NW area suggests mineralization zones where further exploration should be focused.

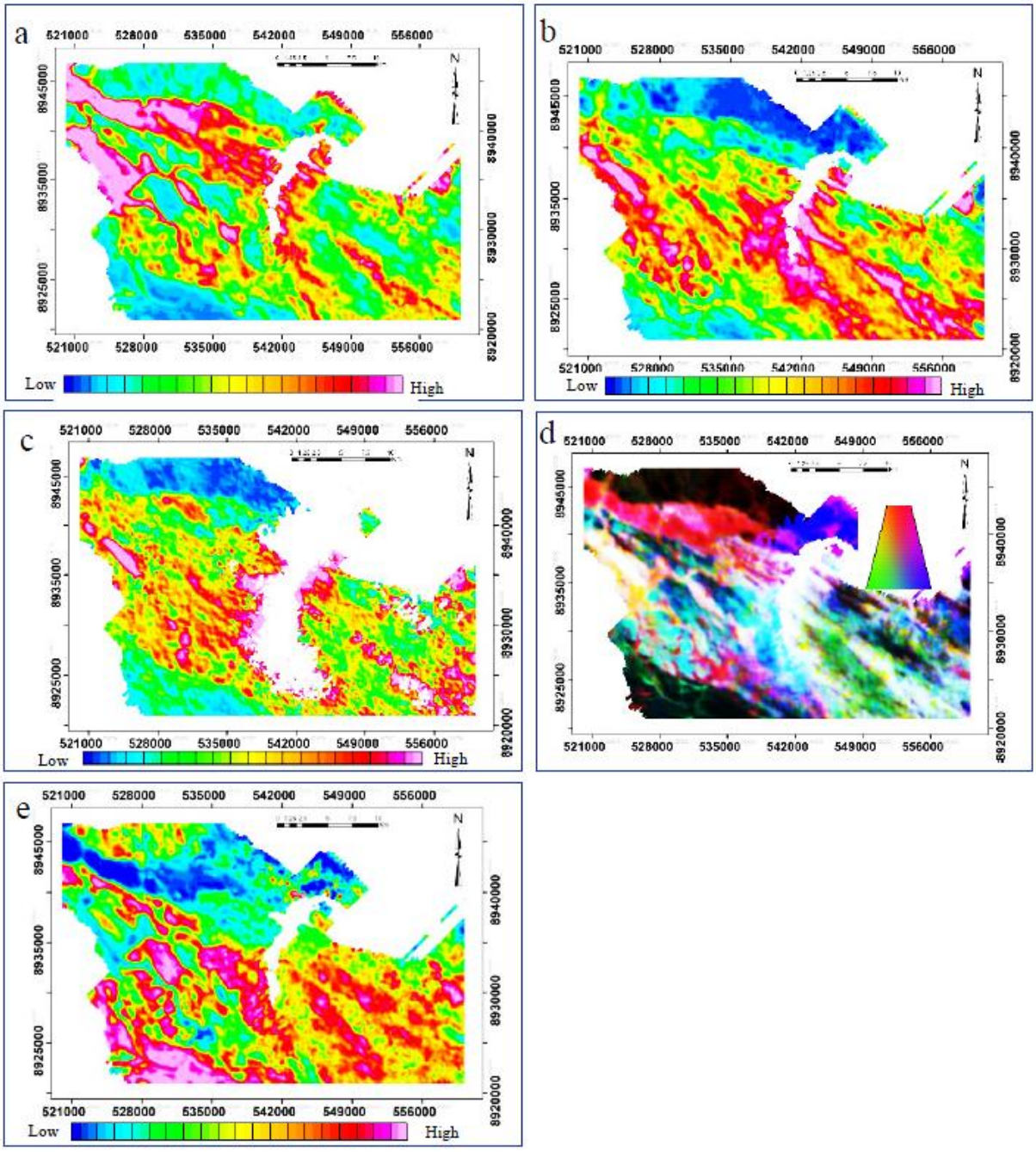

Figure 4. Gamma-ray data indicating (a) Potassium map, (b) Thorium map (c) Uranium map and (d) Ternary map, and (e) Thorium over potassium ratio depicting hydrothermal altered area in blue.

Conflicts of Interest

The researcher declares no conflict of interest

Funding Statement Acknowledgments

We would like to thank the Geological Survey of Malawi for proving data used in the research.

REFERENCES

[1] R. J. Goldfarb and D. I. Groves, "Orogenic gold: Common or evolving fl uid and metal sources through time," Lithos, vol. 233, pp. 2–26, 2015, doi: 10.1016/j.lithos.2015.07.011.

[2] R. J. Goldfarb and D. I. Groves, "Orogenic gold : Common or evolving fl uid and metal sources through time," Lithos, vol. 233, pp. 2–26, 2015, doi: 10.1016/j.lithos.2015.07.011.

[3] R. J. Goldfarb, D. I. Groves, and S. Gardoll, "Orogenic gold and geologic time: a global synthesis," Ore Geol Rev, 2001.

[4] H. Saibi, M. Azizi, and S. Mogren, "Structural Investigations of Afghanistan Deduced from Remote Sensing and Potential Field Data," Acta Geophysica, vol. 64, no. 4, pp. 978–1003, 2016, doi: 10.1515/acgeo-2016-0046.

[5] H. Mohamed et al., "3-D magnetic inversion and satellite imagery for the Um Salatit gold occurrence, Central Eastern Desert, Egypt," Arabian Journal of Geosciences, vol. 11, no. 21, 2018, doi: 10.1007/s12517-018-4020-6.

[6] N. M. Saadi, E. Aboud, H. Saibi, and K. Watanabe, "Integrating data from remote sensing, geology and gravity for geological investigation in the tarhunah area, Northwest libya," Int J Digit Earth, vol. 1, no. 4, pp. 347–366, 2008, doi: 10.1080/17538940802435844.

[7] M. Bersi, H. Saibi, and M. C. Chabou, "Aerogravity and remote sensing observations of an iron deposit in Gara Djebilet, southwestern Algeria," Journal of African Earth Sciences, vol. 116, pp. 134–150, 2016, doi: 10.1016/j.jafrearsci.2016.01.004.

[8] M. Azizi, H. Saibi, and G. R. J. Cooper, "Mineral and structural mapping of the Aynak-Logar Valley (eastern Afghanistan) from hyperspectral remote sensing data and aeromagnetic data," Arabian Journal of Geosciences 2015 8:12, vol. 8, no. 12, pp. 10911–10918, Jun. 2015, doi: 10.1007/S12517-015-1993-2.

[9] M.N. Nabighian, "The analytic signal of two-dimensional magnetic bodies with polygonal cross-section: its properties and use for automated anomaly interpretation.," Geophysics 37, 507±517., 1972.

[10] J. B. Pendry, A. J. Holden, D. J. Robbins, and W. J. Stewart, "Magnetism from conductors and enhanced nonlinear phenomena," IEEE Trans Microw Theory Tech, vol. 47, no. 11, pp. 2075–2084, 1999, doi: 10.1109/22.798002.

[11] A. M. Eldosouky and S. O. Elkhateeb, "Texture analysis of aeromagnetic data for enhancing geologic features using co-occurrence matrices in Elallaqi area, South Eastern Desert of Egyp," NRIAG Journal of Astronomy and Geophysics, vol. 7, no. 2018, pp. 155–161, 2018.

[12] K. O. Olomo, S. Bayode, O. A. Alagbe, G. M. Olayanju, and O. K. Olaleye, "Aeromagnetic Mapping and Radioelement Influence on Mineralogical Composition of Mesothermal Gold Deposit in Part of Ilesha Schist Belt, Southwestern Nigeria," NRIAG Journal of Astronomy and Geophysics, vol. 11, no. 1, pp. 177–192, Dec. 2022, doi: 10.1080/20909977.2022.2057147.

[13] E. M. Schetselaar, J. R. Harris, T. Lynds, and E. A. De Kemp, "Remote Predictive Mapping (RPM): A Strategy for Geological Mapping of Canada North," Journal of geoscience, canada, vol. 34, no. December, pp. 93–111, 2007.

[14] A. A. Komolafe, Z. N. Kuria, T. Woldai, M. Noomen, A. Yekini, and B. Anifowose, "Integrated Remote Sensing and Geophysical Investigations of the Geodynamic Activities at Lake Magadi, Southern Kenyan Rift," vol. 2012, 2012, doi: 10.1155/2012/318301.

[15] A. D. Palomera, "Application of Remote Sensing and Geographic Information Systems for Mineral Predictive Mapping , Deseado Massif , Southern Argentina by," University of Twente, ITC Thesis, 2004.

[16] P. Behnia, J. R. Harris, R. H. Rainbird, M. C. Williamson, and M. Sheshpari, "Remote predictive mapping of bedrock geology using image classification of Landsat and SPOT data, western Minto Inlier, Victoria Island, Northwest Territories, Canada," Int J Remote Sens, vol. 33, no. 21, pp. 6876–6903, Nov. 2012, doi: 10.1080/01431161.2012.693219.

[17] M.-L. Airo and K. Loukola-Ruskeeniemi, "Characterization of sulfide deposits by airborne magnetic and gamma-ray responses in eastern Finland," Ore Geol Rev, vol. 24, no. 1–2, pp. 67–84, Jan. 2004, doi: 10.1016/j.oregeorev.2003.08.008.

[18] M.-L. Airo and M. Wennerström, "Application of regional aeromagnetic data in targeting detailed fracture zones," J Appl Geophy, vol. 71, no. 2–3, pp. 62–70, Jun. 2010, doi: 10.1016/j.jappgeo.2010.03.003.

[19] M.-L. Airo and K. Loukola-Ruskeeniemi, "Characterization of sulfide deposits by airborne magnetic and gamma-ray responses in eastern Finland," The leading Edge, vol. 24, no. 1–2, pp. 67–84, Jan. 2004, doi: 10.1016/j.oregeorev.2003.08.008.

[20] R. T. Ranganai, K. A. Whaler, and C. J. Ebinger, "Aeromagnetic interpretation in the south central Zimbabwe Craton : (reappraisal of) crustal structure and tectonic implications," International Journal of Earth Sciences, pp. 2175–2201, 2015, doi: 10.1007/s00531-015-1279-7.

[21] B. L. Dickson and K. M. Scott, "Interpretation of aerial gamma-ray surveys-adding the geochemical factors," Journal of Australian geology and geophysics, vol. 17, no. 2, pp. 187–200, 1997.

[22] E. Sayed and I. Selim, "The use of magnetic and geo-electrical data to delineate the subsurface structures and groundwater potentiality in Southeastern Sinai, Egypt," Springer, pp. 1479–1494, 2013, doi: 10.1007/s12665-013-2234-1.

[23] P. Keating and M. Pilkington, "Euler deconvolution of the analytic signal and its application to magnetic interpretation," pp. 165–182, 2004.

[24] P. Boszczuk, L. Zhen, P. Roy, S. Lacroix, and A. Cheilletz, "A 3D gravity data interpretation of the Matagami mining camp , Abitibi Subprovince , Superior Province , Québec , Canada Application to VMS deposit exploration," vol. 75, pp. 77–86, 2011, doi: 10.1016/j.jappgeo.2011.06.031.

[25] I. M. Gaafar, "Geophysical signature of the vien-type uranium mineralization of Wadi Eishimbai , Southern Eastern Desert ," pp. 1185–1197, 2012, doi: 10.1007/s12517-010-0263-6.

[26] J. Wang et al., "Lithologic mapping test for gravity and magnetic anomalies A case study of gravity – magnetic anomaly pro fi le in the eastern segment of the China – Mongolia border," J Appl Geophy, vol. 117, pp. 23–31, 2015, doi: 10.1016/j.jappgeo.2015.03.020.

[27] R. B. K. Shives, B. W. Charbonneau, and K. L. Ford, "The detection of potassic alteration by gamma ray spectrometry - recognition of alteration related to mineralization," Radiation Geophysics, no. 416, pp. 1–17, 1997.

[28] M. A. El-sadek, "Radiospectrometric and magnetic signatures of a gold mine in Egypt," J Appl Geophy, vol. 67, no. 1, pp. 34–43, 2009, doi: 10.1016/j.jappgeo.2008.08.012.

[29] S. Herbert, T. Woldai, M. Carranza, and F. J. A. Van Ruitenbeek, "Predictive mapping of prospectivity for orogenic gold in Uganda," Journal of African Earth Sciences, 2014, doi: 10.1016/j.jafrearsci.2014.03.001.

[30] J. Chisambi, T. Haundi, and G. Tsokonombwe, "Geologic structures associated with gold mineralization in the Kirk Range area in Southern Malawi," Open Geosciences, vol. 13, no. 1, pp. 1345–1357, 2021, doi: 10.1515/geo-2020-0304.

[31] S. Ahmed et al., "Magnetic properties of Co doped WSe2 by implantation," J Alloys Compd, vol. 731, pp. 25–31, Jan. 2018, doi: 10.1016/J.JALLCOM.2017.09.288.

[32] K. Bloomfield. and M.S.Garson. "The Geology of the Kirk Range-Lisungwe Valley Area. Ministry of Natural Resources. Geological Survey Department. Bulletin No.17.," The Government Printer, Zomba. Malawi, 1965.

[33] G. S. Cater and J. D. Bennet, The Geology and Mineral Resources of Malawi. Zomba: Government print, Zomba, Malawi, 1973.

[34] Z. Dulanya, "A review of the geomorphotectonic evolution of the south Malawi rift," Journal of African Earth Sciences, 2017.

[35] Z. Dulanya, N. Morales-simfors, and Å. Sivertun, "Journal of African Earth Sciences Comparative study of the silica and cation geothermometry of the Malawi hot springs : Potential alternative energy source," Journal of African Earth Sciences, vol. 57, no. 4, pp. 321–327, 2010, doi: 10.1016/j.jafrearsci.2009.11.001.

[36] U. Ring and A. Kronner, "Shear-zone patterns and eclogite-facies metamorphism in the Mozambique belt of northern Malawi, east-central Africa : implications for the assembly of Gondwana," Precambrian Res, vol. 116, pp. 19–56, 2002.

[37] H. Sommer et al., "Metamorphic petrology and zircon geochronology of high-grade rocks from the central Mozambique Belt of Tanzania : crustal recycling of Archean and Palaeoproterozoic material during the Pan-African orogeny," Journal of Metamorphic Geology, pp. 915–934, 2003, doi: 10.1046/j.1525-1314.2003.00491.x.

[38] N. Boniface, V. Schenk, and P. Appel, "Mesoproterozoic high-grade metamorphism in pelitic rocks of the northwestern Ubendian Belt : Implication for the extension of the Kibaran intra-continental basins to Tanzania," Precambrian Res, vol. 249, pp. 215–228, 2014, doi: 10.1016/j.precamres.2014.05.010.

[39] R. B. McConnell, Outline of the geology of Ufipa and Ubende. Bulletin of Geological Survey of Tanganyika. 1950.

[40] U. Ring, A. Kröner, and T. Toulkeridis, "Palaeoproterozoic granulite-facies meta-morphism and granitoid intrusions in the Ubendian-Usagaran Orogen ofnorthern Malawi, east-central Africa.," Precambrian Reserch., vol. 85, 27–51., 1997.

[41] B. De Waele, J. Liegeois, A. A. Nemchin, and F. Tembo, "Isotopic and geochemical evidence of proterozoic episodic crustal reworking within the irumide belt of south-central Africa , the southern metacratonic boundary of an Archaean Bangweulu Craton," Precambrian Res, vol. 148, pp. 225–256, 2006, doi: 10.1016/j.precamres.2006.05.006.

[42] E. H. Ackermann and A. Forster, "Grundzuge der Stratigraphie und Struktur des Irumide Orogen.," 21st International Geological Congress,. pp. 182–192, 1960.

[43] E. H. Ackermann, "Ein neuer Faltengürtel in Nordrhodesien und seine tektonische Stellung im Afrikanischen Grundgebirge.," Geologische Rundschau, vol. 38, 24–39, 1950.

[44] P. H. Macey et al., "Geology of the Monapo Klippe, NE Mozambique and its significance for assembly of central Gondwana," Precambrian Res, vol. 233, pp. 259–281, 2010, doi: 10.1016/j.precamres.2013.03.012.

[45] R. Boyd et al., "The Geology And Geochemistry Of The East African Orogen In Northeastern Mozambique," Geological Society of South Africa, vol. 113, pp. 87–129, 2010, doi: 10.2113/gssajg.113.1.87.

[46] B. De Waele, I. C. W. Fitzsimons, F. Tembo, and B. Mapani, "The geochronological framework of the Irumide Belt : A prolonged crustal history along the margin of the Bangweulu Craton," Am J Sci, no. February, 2009, doi: 10.2475/02.2009.03.

[47] B. De Waele, "Untying the Kibaran knot : A reassessment of Mesoproterozoic correlations in southern Africa based on SHRIMP U-Pb data from the Irumide belt," Geological Society Of America, no. 6, pp. 509–512, 2003.

[48] H. Sommer and A. Kröner, "Lithos Ultra-high temperature granulite-facies metamorphic rocks from the Mozambique belt of SW Tanzania AR," Lithos, vol. 170–171, pp. 117–143, 2013, doi: 10.1016/j.lithos.2013.02.014.

[49] U. Ring and A. Kronner, "Shear-zone patterns and eclogite-facies metamorphism in the Mozambique belt of northern Malawi, east-central Africa : implications for the assembly of Gondwana," Precambrian Res, vol. 116, pp. 19–56, 2002.

[50] A. Kroner and A. S. Collins, "The East African Orogen: New Zircon and Nd Ages and Implications for Rodinia and Gondwana Supercontinent Formation and Dispersal," Gondwana Research, no. 2, pp. 179–181, 2001.

[51] V. Baranov and H. Naudy, "Numerical Calculation Of The Formula Of Reduction To The Magnetic Pole," Geophysics, vol. 29, no. 1. pp. 67–79, 1964. doi: 10.1190/1.1439334.

[52] Geosoft, "Oasis montaj Viewer 7.0 The core software platform for working with large volume spatial data QUICK STARTTM TUTORIAL." 2008.

[53] A. B. Arogundade, M. O. Awoyemi, O. S. Hammed, S. C. Falade, and O. D. Ajama, "Structural investigation of Zungeru-Kalangai fault zone and its environ, Nigeria using aeromagnetic and remote sensing data," Heliyon, vol. 8, no. 3, p. e09055, Mar. 2022, doi: 10.1016/J.HELIYON.2022.E09055.

[54] A. Ates, F. Bilim, A. Buyuksarac, and Ö. Bektas, "A tectonic interpretation of the Marmara Sea, NW Turkey from geophysical data," Earth, Planets and Space, vol. 60, no. 3, pp. 169–177, 2008, doi: 10.1186/BF03352780.

[55] A. Ateş, A. Büyüksaraç, F. Bilim, Ö. Bektaş, Ç. Şendur, and G. Komanovali, "Spatial correlation of the aeromagnetic anomalies and seismogenic faults in the Marmara region, NW Turkey," Tectonophysics, vol. 478, no. 1–2, pp. 135–142, 2009, doi: 10.1016/j.tecto.2008.09.025.

[56] K. Rozimant, A. Büyüksaraç, and Ö. Bektaş, "Interpretation of magnetic anomalies and estimation of depth of magnetic crust in Slovakia," Pure Appl Geophys, vol. 166, no. 3, pp. 471–484, 2009, doi: 10.1007/s00024-009-0447-8.

[57] C. Reeves, R. Macnab, and S. Maschenkov, "Compiling all the world's magnetic anomalies," Eos, Transactions American Geophysical Union, vol. 79, no. 28, pp. 338–338, Jul. 1998, doi: 10.1029/98EO00255.

[58] N. L. Mohan, W. R. Roest, J. Verhoef, and M. Pilkington, "Magnetic interpretation using the 3-D analytic signal; discussion and reply," Geophysics, vol. 58, no. 8, pp. 1214–1216, Aug. 1993, doi: 10.1190/1.1443507.

[59] F. S. Spector, A. and Grant, "Statistical models for interpreting aeromagneflc data.," Geophysics 35, 293- 302., 1970.

[60] A. M. Aziz, W. A. Sauck, E.-A. H. Shendi, M. A. Rashed, and M. Abd El-Maksoud, "Application of Analytic Signal and Euler Deconvolution in Archaeo-Magnetic Prospection for Buried Ruins at the Ancient City of Pelusium, NW Sinai, Egypt: A Case Study," Surv Geophys, vol. 34, no. 4, pp. 395–411, Apr. 2013, doi: 10.1007/s10712-013-9229-z.

[61] A.B. Reid, J.M., Allsop, H.Granser, A.J. Millett, & I.W. Somerton, "Magnetic interpretation i n three dimensions using Euler deconvolution," Geophysics, vol. v 55, 80-9.

[62] M. Airo and M. Wennerström, "Application of regional aeromagnetic data in targeting detailed fracture zones," J Appl Geophy, vol. 71, no. 2–3, pp. 62–70, 2010, doi: 10.1016/j.jappgeo.2010.03.003.

[63] S. O. Elkhateeb and M. A. G. Abdellatif, "Delineation potential gold mineralization zones in a part of Central Eastern Desert, Egypt using Airborne Magnetic and Radiometric data," NRIAG Journal of Astronomy and Geophysics, vol. 7, no. 2, pp. 361–376, 2018, doi: 10.1016/j.nrjag.2018.05.010.

[64] E. J. Holden, M. Dentith, and P. Kovesi, "Towards the automated analysis of regional aeromagnetic data to identify regions prospective for gold deposits," Comput Geosci, vol. 34, no. 11, pp. 1505–1513, 2008, doi: 10.1016/j.cageo.2007.08.007.

[65] M. Dentith and S. Mudge, Geophysics for Exploration Geoscientist. 2014. doi: 978-0-521-80951-1.

[66] A. B. Reid, J. M. Allsop, H. Granser, A. J. Millett, and I. W. Somerton, "Magnetic interpretation in three dimensions using Euler deconvolution," Geophysics, vol. 55, no. 1, pp. 80–91, Feb. 2012, doi: 10.1190/1.1442774.K. Amponsah-tawiah, "The Mining Industry in Ghana : A Blessing or a Curse.," International Journal of Business and Social Sciences, 2(12), 62–69., 2011.